International Journal of Science Engineering and Advance Technology

Current Control Technique For Grid Connected Distributed Generation (DG) Resources Using ANN controller

[1]Mr. S.Sai Seshu Babu, [2]Mr. S.Shanmukha Sriram
[1]P.G student, [2]ASST.PROF in Dept. of EEE BVC Institute Of Technology And Science, Amalapuram, A.P

Abstract— **This paper deals with the current controlling method based on Artificial Neural Network technique. In this proposed controlling strategy compensation for active, reactive powers will be done and harmonic load current components compensation will be done during connection of DG link to the grid. So that this paper is a multi objective control technique. With this strategy the integration of distributed generation (DG) resources to the electrical power network will get much importance. This proposed control method does not need a phase-locked loop in control circuit and has fast dynamic response in providing active and reactive power components of the grid-connected loads. The transformed variables are used in control of the voltage source converter as the heart of the interfacing system between DG resources and utility grid. Using the compensation current references from the sensed load currents of DG, the active, reactive, and harmonic load current components will be compensated with fast dynamic response, thereby achieving sinusoidal grid currents in phase with load voltages, while required power of the load is more than the maximum injected power of the DG to the grid. The effectiveness of the proposed control technique with ANN controller in DG application are presented using through matlab / simulink software under steady-state and dynamic operating conditions.**

Index Terms— **ANN, distributed generation (DG), renewable energy sources, total harmonic distortion (THD), voltage source converter (VSC).**

I. INTRODUCTION

DG technology can come from conventional technologies such as motors powered by natural gas or diesel fuel or from renewable energy technologies, such as solar PV cells and wind farms. Distributed Generation (DG) technology also known as dispersed generation technology is electricity generating plant connected to a distribution grid rather than the transmission network. There are many types and sizes of DG facilities. These include wind farms, solar photovoltaic (PV) systems, hydroelectric power, or one of the new smaller generation technologies. The DG concept emerged as a way to integrate different power plants, increasing the DG owner's reliability and security, providing additional power quality benefits of the power grid and improving the air quality as a result of lower greenhouse gas emissions of air pollutants. In addition, the cost of the distribution power generation system using the renewable energies is on a falling trend and is expected to fall further as demand and production increase. Over the past two decades, declines in the costs of small scale electricity generation, increases in the reliability needs of many customers, and the partial deregulation of electricity markets have made DG technology more attractive to businesses and households as a supplement to utility-supplied power.

However, the increasing number of DG units in electrical networks requires new techniques for the operation and management of the power networks in order to maintain or even to improve the power supply reliability and quality in the future. As a consequence, the control of DG unit should be improved to meet the requirements for the electrical network. Therefore, design of a control technique, which considers different situations of the electrical networks, becomes of high interest for interconnection of DG units to the power grid. Numerous control techniques and strategies have been proposed and reported for the control and connection of DG units to the electrical grid. An overview of different control and synchronization techniques for DG systems has been presented. Different hardware structures for the DG system, control strategies for the grid-side converter, and control strategies under fault conditions were addressed. Different implementation techniques like *dq*, stationary, and natural frame control structures were presented, and their major characteristics were pointed out. A discussion about different controllers in DG system and their ability to compensate low-order harmonic components presented in the utility grid was given. Finally, an overview of grid synchronization strategies, their influences, and roles in the control of DG system on normal and faulty grid conditions were discussed. A control concept was proposed that provides sharing of harmonic load currents between parallel connected converters without mutual communication. In this paper, a converter operates as an active inductor at a certain frequency to absorb the harmonic current components. However, the exact calculation of grid inductance in real-time systems is not simple, and it can deteriorate the performance of the proposed control strategy. The fact that power grids are faced with unexpected and unavoidable disturbances and uncertainties complicates the design of a practical plug-and play converter-based DG interface.

A robust interfacing scheme for DG converters featuring robust mitigation of converter grid resonance at parameter variation, grid-induced distortion, and current-control parametric instabilities is presented. To ensure high disturbance rejection of grid distortion, converter resonance at parameter variation, and parametric instabilities, an adaptive internal model for the capacitor voltage and grid side current dynamics is included within the current-feedback structure. A control algorithm of three-phase

voltage source converter (VSC) has been proposed for integration of renewable energy resources to the main grid through an output *L*-type or *LCL*-type filter. The proposed controller provides active damping of the *LCL* resonance mode, robustness with respect to grid frequency, and impedance uncertainty. A control technique is proposed to determine which power lines should be inserted into the power network to optimize voltage profile during the presence of DG. An algorithm is suggested in order to design feasible line drop compensation parameters. This algorithm guarantees the satisfaction of voltage constraints for all possible variations in DG output. DG unit was modelled as a PV node, and its control was coordinated with existing volt/var controls to minimize distribution losses. a centralized control algorithm is proposed to operate the control devices using a communication. The proposed control technique aims that active control of DG output and volt/var regulators are in desirable level in order to allow for higher levels of distributed resource integrations. A loss reduction and approximate power flow formula were suggested in the search for optimal feeder configuration for loss minimization. The impact of DG technology on distribution feeder reconfiguration was described.

Several other control strategies of interfacing system between DG resources and electrical grid proposed and presented for different objectives. In all the proposed methods, a solution has been proposed for an important problem in electrical networks. In this paper, a design of a multipurpose control strategy for VSC used in DG system. The idea is to integrate the DG resources to the power grid. With the proposed approach, the proposed VSC controls the injected active power flow from the DG source to the grid and also performs the compensation of reactive power and the nonlinear load current harmonics, keeping the grid current almost sinusoidal during connection of extra loads to the grid. The exact feedback linearization theory is applied in the design of the proposed controller. This control technique allows the decoupling of the currents and enhances their tracking of the fast change in the active and reactive power. This paper shows the complete simulation validation of the proposed method for all its features, i.e., active and reactive power generation along with current harmonic compensation. The simulation results are presented for the grid-connected VSC that generates maximum active power of DG source and compensates for unwanted reactive and harmonic load current component nonlinear loads, thus achieving complete power quality features.

II. PROPOSED DG MODEL

Fig. 1 shows the schematic diagram of the proposed system. Conventional signs of voltages and currents components are also indicated in this schema, where *Rc* and *Lc* represent the equivalent resistance and inductance of the ac filter, coupling transformer, and connection cables; *Rs* and *Ls* represent the grid resistance and inductance up to the point of common coupling (PCC), respectively; *vk* (*k* = 1, 2, 3) is the supply voltage components at the PCC; *vsk* is the grid voltage components; *v*dc is the dc-link voltage; and *isk*, *ilk*, and *ick* are grid, load, and DG current components, respectively. In addition, the DG resources and additional components are represented as a dc current source which is connected to the dc side of the converter.

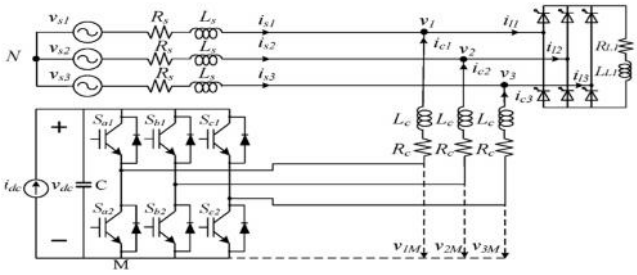

Fig. 1 Schematic diagram of the proposed DG system

III. VOLTAGE AND CURRENT COMPONENTS IN THE SPECIAL REFERENCE FRAMES

The proposed control technique in this paper is based on the analysis of voltage and current vector components in the special reference frames, e.g., 123(abc) to *αβ* and *αβ* to *dq* transformation. The Clarke transformation maps the three phase instantaneous voltages and currents in the 123 phases into the instantaneous voltages and currents on the *αβ*-axes. In the next step, the *αβ* reference frame is transformed to the rotating synchronous reference frame, i.e., in *dq*-components. The synchronous reference frame uses a reference frame transformation module, to transform the grid current and voltage waveforms into a reference frame that rotates synchronously with the grid voltage. By means of this, the control variables become dc values; thus, filtering and controlling can be achieved easily.

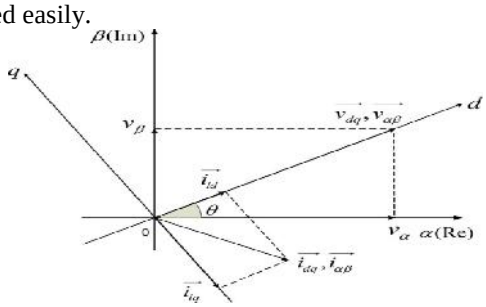

Fig. 2 Voltage and current components in special reference frames

Fig. 2 shows the voltage and current components in *αβ* and *dq* reference frames. Considering *d*-axis vector in the direction of voltage vector in this transformation, the *q*-component of voltage in rotating synchronous reference frame is always zero (*vq* = 0). Therefore, the instantaneous angle of grid voltage can be calculated as

$$\theta = \tan^{-1}\frac{v_\beta}{v_\alpha}. \qquad (1)$$

In other words, if we consider the instantaneous angle of load voltage by (1), the reference voltage vector will be in the direction of *d*-axis vector of load voltage, and *q*-axis vector of load voltage will be zero. According to Fig. 2, the magnitude of the voltage at the PCC can be calculated as

$$v_{\text{ref}} = |\overrightarrow{v_d}| = |\overrightarrow{v_{dq}}| = |\overrightarrow{v_{\alpha\beta}}| = \sqrt{v_\alpha^2 + v_\beta^2}. \qquad (2)$$

In the next stage, reference currents of the DG control loop must be calculated according to the objectives of the proposed DG model.

A. Calculation of Reference Current to Supply Load Active Power

In fundamental frequency, the active power injected from DG link to the grid is

$$P = \frac{3}{2}(v_d I_{cd} + v_q I_{cq}) \quad (3)$$

where capital letters are related to fundamental frequency of the currents. Therefore, by considering the first assumption (vq = 0), d-component of reference current to provide active current in fundamental frequency can be calculated by

$$I^*_{cd} = \frac{2}{3}\frac{P_{\text{ref}}}{v_d} \quad (4)$$

where Pref is maximum power of the VSC in fundamental frequency and I^*_{cd} is the d-component of DG link reference current in fundamental frequency. Due to limited output power of proposed VSC, reference current must be restricted. Calculation of d-component of reference current with this method makes it possible to control the maximum active power injection into the grid by changing Pref. Pref depends on DG system capacity, capacity of power electronic interfacing devices and transformers.

B. Calculation of Harmonic Components of d-Axis Reference Current

In the dq reference frame, the fundamental current component can be seen as a dc component, and as a consequence, the harmonic load currents can be extracted with high-pass filters (HPFs). The main problem with this method is the delay that occurs when the control system is digitally implemented. To minimize the influence of the HPF phase responses, by means of a low-pass filter (LPF), a minimal phase HPF (MPHPF) can be obtained, and the transfer function of this LPF has order and cut-off frequency as the same as HPF. Thus, the MPHPF can be obtained simply by the difference between the input signal and the filtered one, which is equivalent to performing $H_{\text{MPHPF}}(s) = 1 - H_{\text{LPF}}(s)$. A double-precision filter using the Chebyshev type-II fifth-order LPF is used for this purpose. The filter considered has a cut-off frequency $fc = (f/2)(f = 50$ Hz) which promises the extraction of dc components in the nonlinear load currents. Therefore, i_{ld} can be expressed as

$$i_{ld} = \tilde{i}_{ld} + I_{ld} \quad (5)$$

Where $i\wedge_{ld}$ is alternative d-component of load current which is related to harmonic components of load current and I_{ld} is the dc term of load current which is related to fundamental frequency of load current. To use DG link as an active power filter, harmonic components of the nonlinear load current must be supplied. For this purpose, d-component of nonlinear link reference current is achieved by doing the sum of currents in (4) and alternative terms of load current in (5)

$$i^*_{cd} = \tilde{i}_{ld} + \dot{I}\,cd. \quad (6)$$

C. Calculation of Reference Current to Supply Load Reactive Power

In dq frame, quadrature component of load current is perpendicular to direct component of voltage ($v_d \perp i_{lq}$). As a result, q-component of load current indicates required reactive power of the load. To compensate load reactive power, DG must provide a current with q-component equal to i_{lq}. For this purpose, it is sufficient to set q-component of DG's reference current equal to q-component of the load current as

$$i^*_{cq} = i_{lq}. \quad (7)$$

The term of i^*_{cq} is the q-component of DG link reference current. By this consideration, total load reactive current and harmonic components of q-axis are compensated.

IV. MODELING OF THE PROPOSED DG SYSTEM

For the purposes of this paper, the electric power grid is composed of the generation system, the transmission, or the distribution system, and the loads. The DG source and additional components are represented as a dc current source connected to the dc side of the proposed converter. To draw an appropriate plan to control the integration of DG resources to the power grid, a dynamic analytical model of the proposed power system should be developed.

A. Proposed Model Analysis

Kirchhoff's laws of voltage and current applied to the proposed model shown in Fig. 1 provide a general equation in the stationary reference frame in a three-phase system as

$$\sum_{i=1}^{3} v_{iM} = \sum_{i=1}^{3}\left(L_c\frac{di_{ci}}{dt} + R_c i_{ci} + v_i + v_{NM}\right). \quad (8)$$

A null value for the zero voltage component is assumed. Since the absence of neutral wire is considered, the zero current component is also null, with the assumption that the grid voltages are balanced. By taking into account these assumptions, the ac neutral point voltage term can be obtained as

$$v_{NM} = \frac{(v_{1M} + v_{2M} + v_{3M})}{3} = \frac{1}{3}\sum_{i=1}^{3} v_{iM}. \quad (9)$$

The switching function s_k of the k_{th} leg of the VSC can be expressed as

$$S_k = \begin{cases} 1, & \text{if } T_k \text{ is on and } T'_k \text{ is off} \\ 0, & \text{if } T_k \text{ is off and } T'_k \text{ is on.} \end{cases} \quad (10)$$

Thus, with $vkM = S_k v_{\text{dc}}$ and substituting in (8) and (9), a set of dynamic equations describing the switched model of the proposed DG model is developed. This model is general, complete, and makes no assumptions other than the use of ideal switches. Therefore, (11) can be expressed as

$$\frac{di_{ck}}{dt} = -\frac{R_c}{L_c}i_{ck} + \frac{1}{L_c}\left(S_k - \frac{1}{3}\sum_{j=1}^{3} S_j\right)v_{\text{dc}} - \frac{v_k}{L_c}$$

$$k = 1, 2, 3. \quad (11)$$

Equation (11) represents phase k dynamic equation of the proposed VSC. By (11), the switching state function can be defined as

$$D_{nk} = \left(S_k - \frac{1}{3}\sum_{j=1}^{3} S_j\right). \quad (12)$$

Equation (12) shows that the value of Dnk depends on the switching state n and on the phase k. In other words, Dnk depends simultaneously on the switching functions of the three legs of the interfaced VSC. This shows the interaction between the three phases.

By substituting (12) into (11), dynamic equation of the proposed model can be expressed as

$$\frac{d}{dt}\begin{bmatrix} i_{c1} \\ i_{c2} \\ i_{c3} \end{bmatrix} = -\frac{R_c}{L_c}\begin{bmatrix} 1 & 0 & 0 \\ 0 & 1 & 0 \\ 0 & 0 & 1 \end{bmatrix}\begin{bmatrix} i_{c1} \\ i_{c2} \\ i_{c3} \end{bmatrix} + \frac{1}{L_c}\begin{bmatrix} D_{n1} \\ D_{n2} \\ D_{n3} \end{bmatrix} v_{\rm dc} - \frac{1}{L_c}\begin{bmatrix} v_1 \\ v_2 \\ v_3 \end{bmatrix}. \quad (13)$$

V. STATE-SPACE MODEL OF PROPOSED SYSTEM

By use of Park transformation matrix, the dynamic equation of proposed model can be transformed to the *dq* frame as

$$\frac{d}{dt}\begin{bmatrix} i_{cd} \\ i_{cq} \end{bmatrix} = \begin{bmatrix} -\frac{R_c}{L_c} & \omega \\ -\omega & -\frac{R_c}{L_c} \end{bmatrix}\begin{bmatrix} i_{cd} \\ i_{cq} \end{bmatrix} + \frac{1}{L_c}\begin{bmatrix} D_{nd} \\ D_{nq} \end{bmatrix} v_{\rm dc} - \frac{1}{L_c}\begin{bmatrix} v_d \\ v_q \end{bmatrix}. \quad (14)$$

As the sum of the three-phase currents is zero, there is no homopolar component ($ic0 = 0$); therefore, the ac neutral point voltage does not affect any transformed current. This voltage can be deduced as

$$v_{NM} = \frac{v_0 - v_{0M}}{\sqrt{3}}. \quad (15)$$

It can be seen that the v_{NM} only depends on homopolar voltage components of the converter (v_{0M}) and the grid (v_0). In addition, when the voltage of power grid is balanced, the averaged value of v_0 is zero; therefore, voltage v_{NM} depends only on the homopolar component of the ac voltages of the interfaced converter. Considering the original position of the load voltage vector in *d*-axis, voltage vector of *q*-axis will be zero ($v_q = 0$), and the other vector's value will be equal to *EL* ($v_d = E_L$), which is the value of the line-to-line rms voltage of grid voltage. Therefore, (14) can be written as

$$\frac{d}{dt}\begin{bmatrix} i_{cd} \\ i_{cq} \end{bmatrix} = \begin{bmatrix} -\frac{R_c}{L_c} & \omega \\ -\omega & -\frac{R_c}{L_c} \end{bmatrix}\begin{bmatrix} i_{cd} \\ i_{cq} \end{bmatrix} + \frac{1}{L_c}\begin{bmatrix} D_{nd} \\ D_{nq} \end{bmatrix} v_{\rm dc} - \frac{1}{L_c}\begin{bmatrix} E_L \\ 0 \end{bmatrix} \quad (16)$$

where the homopolar component has been omitted.

A. Current Control Technique using PI controller:

In order to obtain a low overshoot, high accuracy, and fast dynamic response to provide load active and reactive power and also harmonic current components of the grid-connected loads, two equations in the equivalent model of the proposed system (14) must be controlled in two different and independent loops. As we mentioned before, all the Park-transformed variables of the DG system will become a constant value in steady-state condition. By referring to (14) and considering $\lambda = L_c(d_{ic}/dt) + R_c i_c$, switching state functions can be calculated as

$$D_{nd} = \frac{\lambda_d - L_c\omega i_{cq} + v_d}{v_{\rm dc}} \quad (17)$$

$$D_{nq} = \frac{\lambda_q + L_c\omega i_{cd}}{v_{\rm dc}}. \quad (18)$$

As shown in (17) and (18), the cross coupling terms $L_c\omega i_{cq}$ and $L_c\omega i_{cd}$ exist in circuit of current control loop, and the blocks that contain $L_c\omega$ have the objective of decoupling influenced between both current control loops in the *d*- and *q*-axes. Note that the original control inputs D_nd and D_nq consist of combination of a nonlinearity cancelation part and a linear decoupling compensation part. To achieve a fast dynamic response and zero steady-state errors, particularly during connection of nonlinear loads to the grid, which main grid is polluted by these types of loads, a proportional–integral (PI)-type regulator is needed. The parameter of the proposed regulator can be obtained as

$$(\lambda_{dq}) = k_p(\Delta i_{cdq}) + k_i \int (\Delta i_{cdq})\, dt \quad (19)$$

where terms *kp* and *ki* are proportional and integral gains, respectively, and ($\Delta icdq$) = (i^*cdq) − ($icdq$) denotes a comparison of the calculated reference currents and the actual DG injection currents generated by the VSC which create error signals and control the switches of the inverter according to objectives of the interconnection of DG system to the grid. The transfer function of the PI regulator for current control loops of proposed strategy is given as

$$G_i(s) = \frac{\lambda_d(s)}{\Delta I_d(s)} = \frac{\lambda_q(s)}{\Delta I_q(s)} = k_p + \frac{k_i}{s}. \quad (20)$$

To design PI regulator in circuit of current controller, it is necessary to decouple the model of the system by adding the measured voltage of *d*-axis and cross-coupling terms as shown in Fig. 3, where $L*$ and $v*$ are estimated values of coupling inductance and grid voltages.

Thus, the inner control loops of the current *icd* can be simplified as shown in Fig. 4. As shown in Fig. 3, the current loops of *icd* and *icq* are the same. Thus, in *dq* reference frame, decoupled control for the reactive and active power can be conveniently achieved by independently controlling the *d*- and *q*-axis currents.

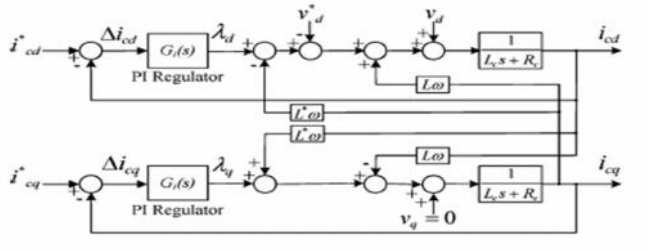

Fig. 3 Inner control loop of the *icd* and *icq*.

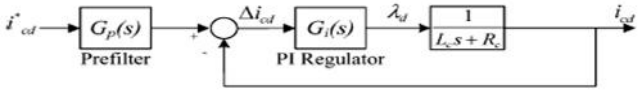

Fig. 4 Equivalent diagram of *d*-axis current control loop

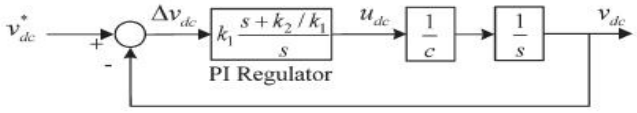

Fig. 5 Control loop of the dc voltage.

The closed-loop transfer function of the current loop can be calculated as

$$\frac{I_{cq}(s)}{I^*_{cq}(s)} = \frac{I_{cd}(s)}{I^*_{cd}(s)} = \frac{k_p}{L_c}\frac{s + \frac{k_i}{k_p}}{s^2 + \frac{(R_c + k_p)}{L_c}s + \frac{k_i}{L_c}}. \quad (21)$$

The transient response of the currents will be affected by the presence of the zero in (21). In particular, the actual percent overshoot will be much higher than expected. For the optimal value of the damping factor $\zeta = \sqrt{1/2}$, the theoretical overshoot is 20.79%. To eliminate the effect of zero on transient response in (21), a prefilter is added as shown in Fig. 4. The response of the current loops becomes that of a second-order transfer function with no zero.

Comparison between general model of a second-order transfer function $\omega^2 n/(s^2 + 2\xi\omega ns + \omega^2 n)$ and (21) leads to the following design relations:

$$k_p = 2L_c\zeta\omega_n - R_c \qquad k_i = L_c \cdot \omega_n^2 \qquad (22)$$

where ω_n is natural undamped angular frequency and depends on the specific time response.

B. Proposed ANN controller:

Many hundreds of Neural Network types have been proposed over the years. In fact, because Neural Nets are so widely studied (for example, by Computer Scientists, Electronic Engineers, Biologists and Psychologists), they are given many different names. They referred to as Artificial Neural Networks (ANNs), Connectionism or Connectionist Models, Multi-layer Percpetrons (MLPs) and Parallel Distributed Processing (PDP).

However, despite all the different terms and different types, there are a small group of "classic" networks which are widely used and on which many others are based. These are: Back Propagation, Hopfield Networks, Competitive Networks and networks using Spiky Neurons. There are many variations even on these themes. We'll consider these networks in this and the following chapters, starting with Back Propagation.

i) The algorithm

Most people would consider the Back Propagation network to be the quintessential Neural Net. Actually, Back Propagation is the training or learning algorithm rather than the network itself. These are called *Feed- Forward* Networks or occasionally *Multi-Layer Perceptrons (MLPs).*

The network operates in exactly the same way as the others we've seen. Now, let's consider what Back Propagation is and how to use it. A Back Propagation network learns by example. You give the algorithm examples of what you want the network to do and it changes the network's weights so that, when training is finished, it will give you the required output for a particular input. Back Propagation networks are ideal for simple Pattern Recognition and Mapping Tasks. The figure 6 shows the single connection learning, in the back propagation network.

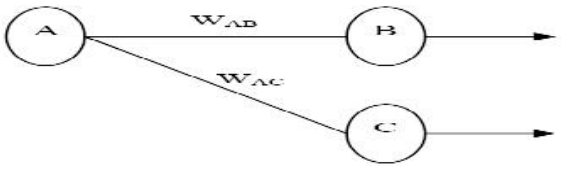

Fig 6 single connection learning in BP network

The connection we're interested in is between neuron A (a hidden layer neuron) and neuron B (an output neuron) and has the weight WAB. The diagram also shows another connection, between neuron A and C, but we'll return to that later. The algorithm works like this:

1. First apply the inputs to the network and work out the output – remember this initial output could be anything, as the initial weights were random numbers.

2. Next work out the error for neuron B. The error is *what you want – What you actually get*, in other words:

Error B = Output B (1-Output B) (Target B – Output B)

The "*Output (1-Output)*" term is necessary in the equation because of the Sigmoid Function – if we were only using a threshold neuron it would just be *(Target – Output).*

3. Change the weight. Let W+AB be the new (trained) weight and WAB be the initial weight.

W+AB = WAB + (Error B x Output A)

Notice that it is the output of the connecting neuron (neuron A) we use (not B). We update all the weights in the output layer in this way.

4. Calculate the Errors for the hidden layer neurons. Unlike the output layer we can't calculate these directly (because we don't have a Target), so we *Back Propagate* them from the output layer (hence the name of the algorithm). This is done by taking the Errors from the output neurons and running them back through the weights to get the hidden layer errors. For example if neuron A is connected as shown to B and C then we take the errors from B and C to generate an error for A.

Error A = Output A (1 - Output A)(Error B WAB + Error C WAC)

Again, the factor "*Output (1 - Output)*" is present because of the sigmoid squashing function.

5. Having obtained the Error for the hidden layer neurons now proceed as in stage 3 to change the hidden layer weights. By repeating this method we can train a network of any number of layers.

VI. DC VOLTAGE REGULATION

The error value of the dc-bus voltage $\Delta v_{dc} = v^*_{dc} - v_{dc}$ is passed through a PI-type compensator to regulate the voltage of dc bus (v_{dc}) at a fixed value. Therefore, u_{dc} will be obtained as

$$u_{dc} = k_1 \Delta v_{dc} + k_2 \int \Delta v_{dc}\, dt \qquad (23)$$

where $k1$ and $k2$ are proportional and integral gains of the proposed PI regulator. Fig. 5 shows the equivalent control circuit loop of the dc-bus voltage for proposed converter. The closed-loop transfer function of the proposed dc voltage regulation loop, got from Fig. 5, has the following form:

$$\frac{v_{dc}(s)}{v^*_{dc}(s)} = 2\zeta\omega_{nv}\frac{s + \frac{\omega_{nv}}{2\zeta}}{s^2 + 2\zeta\omega_{nv}s + \omega_{nv}^2} \qquad (24)$$

where the proportional and integral gains are derived from

$$k_1 = 2\zeta\omega_{nv}C \qquad k_2 = \omega_{nv}^2 C. \qquad (25)$$

The control effort is obtained from

$$i^*_{do} = \frac{u_{dc} - D_{nq}i_q}{D_{nd}} = \frac{u_{dc}v_{dc} - D_{nq}v_{dc}i_q}{D_{nd}v_{dc}}. \qquad (26)$$

However, assuming that the current loop is ideal and in normal operation of the active filter, the following properties hold, assuming the supply voltages are given by:

$$\begin{aligned} v_1 &= v\cos(\omega t) \\ v_2 &= v\cos(\omega t - 2\pi/3) \\ v_3 &= v\cos(\omega t - 4\pi/3). \end{aligned} \quad (27)$$

The transformation to the synchronous reference frame yields

$$\begin{bmatrix} v_d \\ v_q \end{bmatrix} = T_{dq}^{12}\begin{bmatrix} v_1 \\ v_2 \end{bmatrix} = \sqrt{\frac{3}{2}}\begin{bmatrix} v \\ 0 \end{bmatrix}. \quad (28)$$

As a result, $D_{nq}v_{dc} \approx v_q = 0$ and $D_{nd}v_{dc} \approx v_d = \sqrt{(3/2)}v$.

Hence, the control effort can be approximated by

$$i_{d1h+} \approx \sqrt{\frac{2}{3}}\cdot\frac{v_{dc}}{v}u_{dc}. \quad (29)$$

The reference current in (29) is added to the harmonic reference current of the loop of i_{ld}. i_{d1h+} is a dc component, and it will force the active filter to generate or to draw a current at the fundamental frequency. Furthermore, by designing the dc voltage loop much slower than the current loop, there would not be any interaction between the two loops.

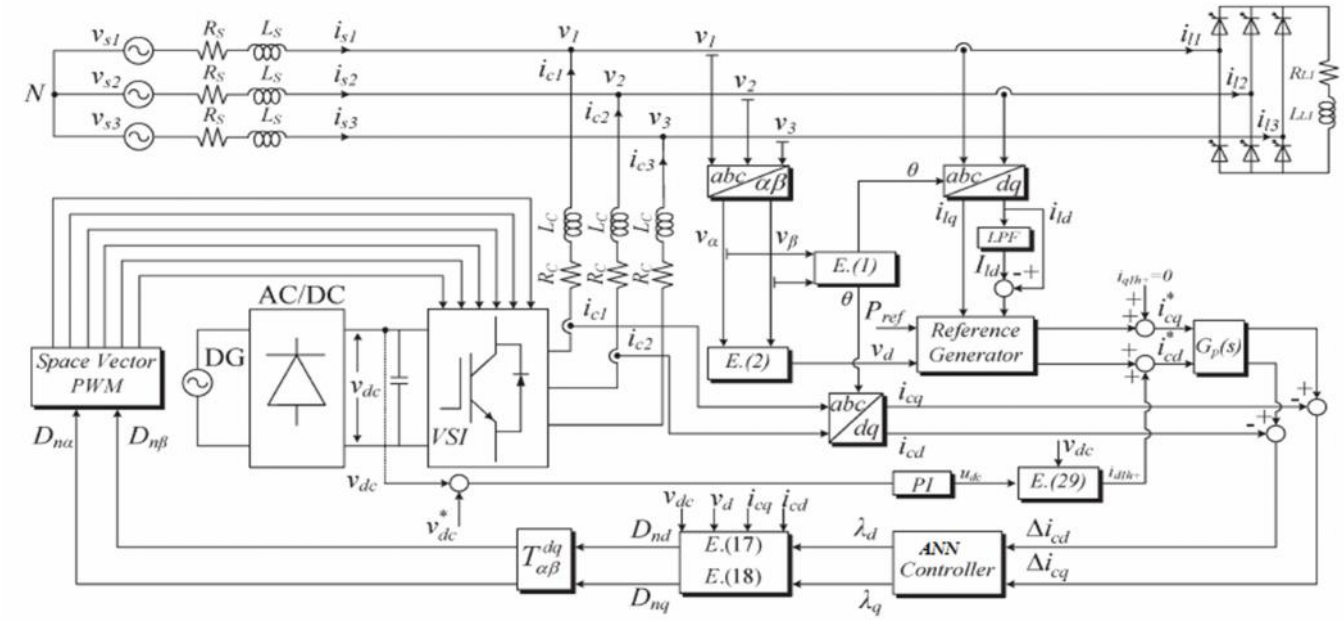

Fig. 8 General schematic diagram of the proposed control strategy with ANN controller

VII. SIMULATION ANALYSIS AND RESULTS

The complete system model was simulated using the "Power System Blockset" simulator operating under the Matlab/Simulink environment. The schematic diagram and principle of the proposed models and the control technique in an ac grid are shown in Fig. 6. The test model contains a power converter with power rating of 20 kVA. The maximum available value of DG source active power is 8 kW, which is also the active power reference included in the simulations. At first, capabilities of DG resources and flexibility of proposed control strategy to control the proposed VSC in providing active, reactive, and harmonic current components of different loads are shown, and the capabilities of proposed control method on reactive power tracking with constant output active power are considered.

Case-1: Simulation results with PI controller

The simulated results have been used to analyze the total harmonic distortion (THD) of the utility grid current amid severe varying load conditions. During the simulation process, constant dc voltage sources have been considered as a DG source. In addition, the active power which is delivered from the DG link to the ac grid is considered to be constant. This assumption makes it possible to evaluate the capability of the proposed control strategy to track the fast change in the active and reactive power, independent of each other. For this purpose, when one of them is changed, another one must be constant. To simulate a real ac grid, the load is connected and disconnected to the power grid randomly, and grid current waveform will be compared with each other under various loads and conditions.

A. Connection of DG Link to the Grid to Supply Harmonic Current Components and Nonlinear Load Increment

A full-wave thyristor converter supplies a load with resistance of 20 Ω and 10-mH inductors in each phase. This nonlinear load draws harmonic currents from the grid continuously. The DG link is connected to the ac grid at t = 0.1 s. This process is continued until t = 0.2; at this moment, another full-wave thyristor converter similar to the prior load is connected to the grid, and it is disconnected from the grid at t = 0.35 s. Fig. 8 shows the load voltage (*vl*), load current (*il*), grid current (*i*grid), and DG current (*i*DG) in phase (a).

ISSN 2321-6905

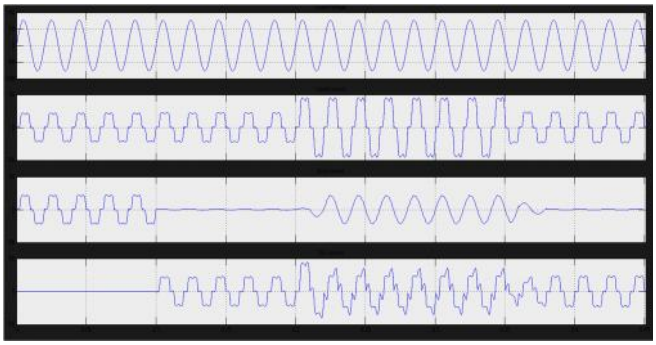

Fig. 8 Load voltage, load, grid, and DG currents before and after connection of DG and before and after connection and disconnection of additional load into the grid

As shown in this figure, after the connection of DG link to the grid at t = 0.1 s, the grid current becomes zero, and all the active and reactive current components including fundamental and harmonic frequencies are provided by DG link ($i$grid = $i$load − iDG). In this case, load current is completely equal to reference current of converter; therefore, VSC injects the maximum available power of DG source to the power grid. As a result, the injected current from the grid will be zero. The load current is fed from nonlinear link continuously until the connection of additional load to the grid.

Fig. 9(a) shows that, after connection of additional load to the power grid at t = 0.2 s, converter injects the maximum active and reactive power by connection of DG source to the grid. However, in this case, the maximum power of proposed converter is less than the power which is needed to supply the grid-connected loads. Therefore, the remaining power is injected by the utility grid. As shown in this figure, the utility grid injects high-power quality current waveforms even under the connection of nonlinear loads to the grid, and load harmonic currents are provided by DG. There are some sharp edges on current waveforms which are related to high-order harmonic frequencies and created during switching of thyristor converters.

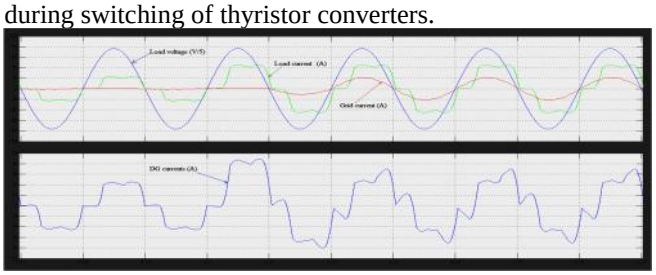

(a)

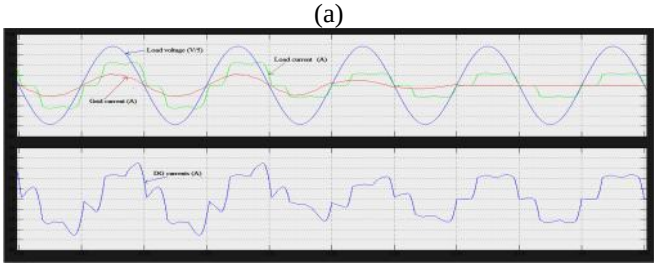

(b)

Fig. 9 Grid, load, DG currents, and load voltage (a) before and after connection of additional load and (b) before and after disconnection of additional load.

In addition, the production in control circuit of DG system is delayed for around one cycle. This is due to the settling time of proposed MPHPF filter, in DG's control loop. Fig. 9(b) shows that, with the same delay as before, additional load is removed at t = 0.35 s. As shown in this figure, after the pass of the transient times, the injected current from grid to the load becomes zero, and DG link supplies all the required power to supply the proposed nonlinear load.

Fig. 10 shows that, after the transient times during connection of additional load to the main grid, the load voltage and grid current are in phase, and the grid does not need to provide reactive and harmonic currents for the load which is shown for three phases.

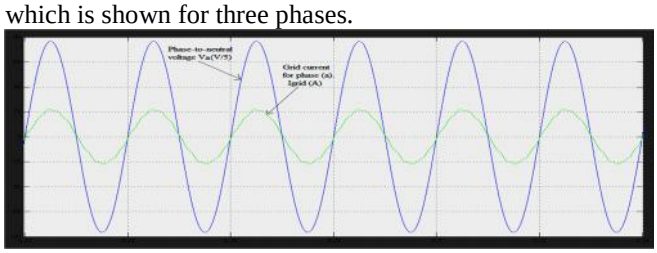

Fig.10 Phase-to-neutral voltage and grid current for phase-A

The ability of control loop to track the reference current trajectories of d- and q-axes, during connection of DG link to the grid and, also, connection of additional load to the grid, is shown in Fig. 11. Fig. 11(a) shows that, before connection of additional load to the grid, the actual d- and q-axis current components of DG's control loop track their reference trajectory precisely. However, according to Fig. 11(b), after connection of additional load to the grid, the actual d-axis current component of DG tracks half of its reference trajectory which is equal to its maximum active power (reference active power), and all the reference trajectories of reactive current change.

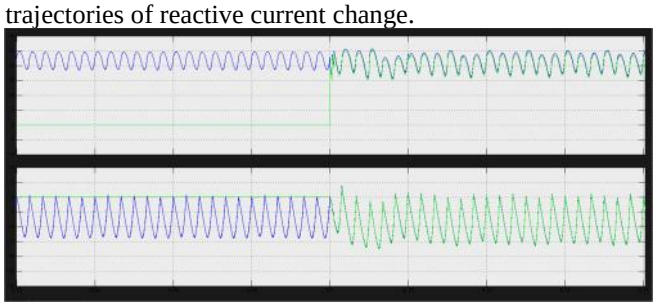

(a)

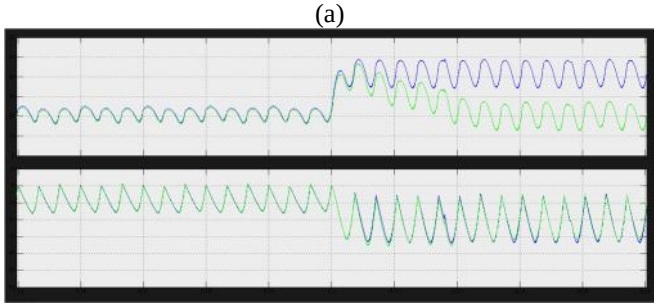

(b)

Fig. 11 Reference currents track the load current (a) after interconnection of DG resources and (b) after additional load increment

B. Connection of DG Link to an Unbalanced Grid

The ability of proposed DG link to track load current components for unbalanced grid voltage is evaluated. At first, a nonlinear load similar to the prior load is added to the PCC at t = 0.45 s. At t = 0.55 s, the grid voltage is unbalanced. Fig. 12 shows three-phase grid voltages, load current, grid current, and DG link current. As shown in Fig. 12, load harmonic current components are provided by DG link, and grid currents are maintained sinusoidal during balanced and unbalanced grid voltages. In addition, load voltage and grid current are kept in phase (the grid does not provide reactive current). The proposed control scheme provides balanced current injection from the DG link. Therefore, since the grid voltage unbalance forces unbalanced current in the load, the grid current is unbalanced. Depending on the power converter current ratings and voltage unbalance severity, it could be possible to compensate the grid currents unbalance by injecting unbalance currents from the DG link, but this is not the purpose of the present control scheme.

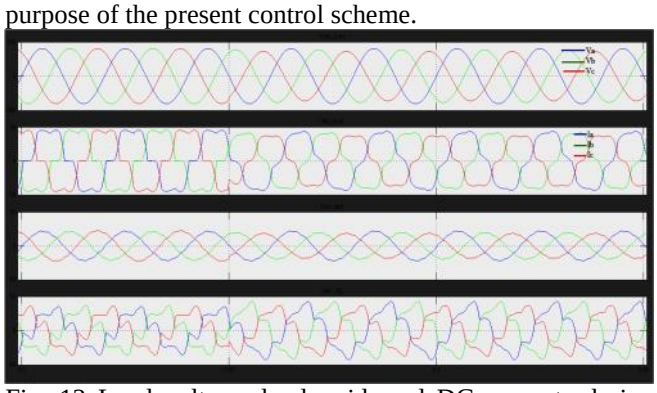

Fig. 12 Load voltage, load, grid, and DG currents during connection of DG link to the unbalanced grid voltage.

Case-2: Simulation results with ANN controller

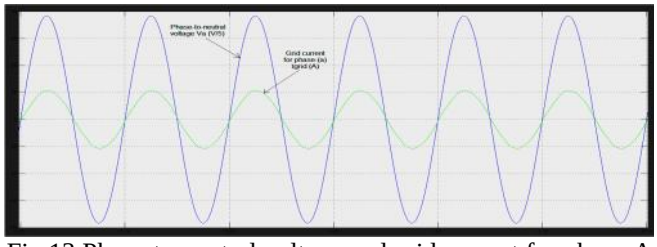

Fig.13 Phase-to-neutral voltage and grid current for phase-A with ANN controller

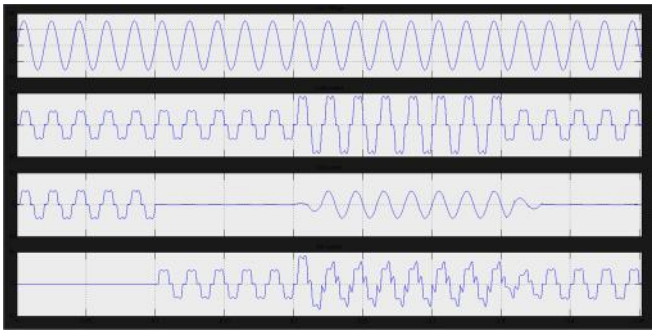

Fig. 14 Load voltage, load, grid, and DG currents before and after connection of DG and before and after connection and disconnection of additional load into the grid using ANN controller

TABLE-I

Comparison between PI & ANN controllers

FUNDAMENTAL AND THD VALUES OF GRID CURRENTS									
Before Compensation				After Compensation PI			After Compensation ANN		
Peak current (A)	Igrid1	Igrid2	Igrid3	Igrid1	Igrid2	Igrid3	Igrid1	Igrid2	Igrid3
Fundamental (50Hz)	36.02	36.02	36.2	21.35	20.93	20.88	21.35	20.93	20.88
THD %	16.48	16.46	16.47	4.74	4.44	4.21	1.62	1.51	1.45

VIII. CONCLUSION

Flexibility of the proposed DG in both steady-state and transient operations has been verified through simulation results. And comparisons are made between PI controller & ANN controller. A multi objective control algorithm for the grid-connected converter-based DG system with PI & ANN controller has been proposed and presented in this paper. One other advantage of proposed control method is its fast dynamic response in tracking reactive power variations; the control loops of active and reactive power are considered independent. By the use of the proposed control method, DG system is introduced as a new alternative for distributed static compensator in distribution network. The results illustrate that, in all conditions, the ANN controller will give good results compared with PI controller. The THD comparison was shown in shown in table-I. The proposed control technique can be used for different types of DG resources as power quality improvement devices in a customer power distribution network.

VI. Acknowledgment

This paper is based on M. Tech. project carried out by the student of BVC Institute of Technology And Science, Amalapuram studying M.Tech (Power System). The project had been completed by Mr. S.SAI SESHU BABU, Mail id: srirangamsaiseshubabu@gmail.com, under the guidance of Mr. S.SHANMUKHA SRIRAM.

TABLE-II

SYSTEM PARAMETERS

Parameter	Value
Grid voltage	230 V
Interfacing inductance	4.6 mH
DC-link capacitance	1020 µF
DC-link voltage setpoint	610 V
Switching/Sampling frequency	10 kHz
Fundamental frequency	50 Hz
Linear load resistance	40 Ω
Linear load inductance	100 mH
Nonlinear load resistance	180 Ω

REFERENCES

[1] E. Pouresmaeil, D. Montesinos-Miracle, O. Gomis-Bellmunt, and J. Bergas-Jané, "A multi-objective control strategy for grid connection of DG (distributed generation) resources," *Energy*, vol. 35, no. 12, pp. 5022–5030, Dec. 2010.

[2] F. Blaabjerg, R. Teodorescu, M. Liserre, and A. V. Timbus, "Overview of control and grid synchronization for

distributed power generation systems," *IEEE Trans. Power Electron.*, vol. 53, no. 5, pp. 1398–1409, Oct. 2006.
[3] F. Blaabjerg, Z. Chen, and S. Kjaer, "Power electronics as efficient interface in dispersed power generation systems," *IEEE Trans. Power Electron.*, vol. 19, no. 5, pp. 1184–1194, Sep. 2004.
[4] G. Saccomando and J. Svensson, "Transient operation of grid-connected voltage source converter under unbalanced voltage conditions," in *Proc. IAS*, Chicago, IL, Oct. 2001, vol. 4, pp. 2419–2424.
[5] R. Teodorescu and F. Blaabjerg, "Flexible control of small wind turbines with grid failure detection operating in stand-alone or grid-connected mode," *IEEE Trans. Power Electron.*, vol. 19, no. 5, pp. 1323–1332, Sep. 2004.
[6] M. Kazmierkowski, R. Krishnan, and F. Blaabjerg, *Control in Power Electronics—Selected Problems*. New York: Academic, 2002.
[7] E. Twining and D. G. Holmes, "Grid current regulation of a three-phase voltage source inverter with an *LCL* input filter," *IEEE Trans. Power Electron.*, vol. 18, no. 3, pp. 888–895, May 2003.
[8] T. Zhou and B. François, "Energy management and power control of a hybrid active wind generator for distributed power generation and grid integration," *IEEE Trans. Ind. Electron.*, vol. 58, no. 1, pp. 95–104, Jan. 2011.
[9] M. Singh, V. Khadkikar, A. Chandra, and R. K. Varma, "Grid interconnection of renewable energy sources at the distribution level with power quality improvement features," *IEEE Trans. Power Del.*, vol. 26, no.1, pp. 307–315, Jan. 11
[10] M. F. Akorede, H. Hizam, and E. Pouresmaeil, "Distributed energy resources and benefits to the environment," *Renewable Sustainable Energy Rev.*, vol. 14, no. 2, pp. 724–734, Feb. 2010.
[11] C. Mozina, "Impact of green power distributed generation," *IEEE Ind. Appl. Mag.*, vol. 16, no. 4, pp. 55–62, Jun. 2010.
[12] B. Ramachandran, S. K. Srivastava, C. S. Edrington, and D. A. Cartes, "An intelligent auction scheme for smart grid market using a hybrid immune algorithm," *IEEE Trans. Ind. Electron.*, vol. 58, no. 10, pp. 4603–4611, Oct. 2011.
[13] E. Twining and D. G. Holmes, "Grid current regulation of a three-phase voltage source inverter with an *LCL* input filter," *IEEE Trans. Power Electron.*, vol. 18, no. 3, pp. 888–895, May 2003.
[14] M. K. Ghartemani and M. Iravani, "A method for synchronization of power electronic converters in polluted and variable-frequency environments," *IEEE Trans. Power Syst.*, vol. 19, no. 3, pp. 1263–1270, Aug. 2004.
[15] U. Borup, F. Blaabjerg, and P. N. Enjeti, "Sharing of nonlinear load in parallel-connected three-phase converters," *IEEE Trans. Ind. Appl.*, vol. 37, no. 6, pp. 1817–1823, Nov./Dec. 2001.
[16] Y. A.-R. I. Mohamed, "Mitigation of grid-converter resonance, gridinduced distortion and parametric instabilities in converter-based distributed generation," *IEEE Trans. Power Electron.*, vol. 26, no. 3, pp. 983–996, Mar. 2011.
[17] H. Karimi, A. Yazdani, and R. Iravani, "Robust control of an autonomous four-wire electronically-coupled distributed generation unit," *IEEE Trans. Power Del.*, vol. 26, no. 1, pp. 455–466, Jan. 2011.
[18] V. Calderaro, V. Galdi, and A. Picolo, "Distribution planning by genetic algorithm with renewable energy units," in *Proc. Bulk Power Syst. Dyn. Control*, Cortina d'Ampezzo, Italy, 2004, vol. 1, pp. 375–380.
[19] M. Kim, R. Hara, and H. Kita, "Design of the optimal ULTC parameters in distribution system with distributed generations," *IEEE Trans. Power Syst.*, vol. 24, no. 1, pp. 297–305, Feb. 2009.
[20] J.-H. Teng, C.-Y. Chen, C.-F. Chen, and Y.-H. Liu, "Optimal capacitor control for unbalanced distribution systems with distributed generations," in *Proc. IEEE ICSET*, Singapore, 2008, pp. 755–760.
[21] H. Hatta, S. Uemura, and H. Kobayashi, "Demonstrative study of control system for distribution system with distributed generation," in *Proc. IEEE/PES Power Syst. Conf. Expo.*, Seattle, WA, 2009, pp. 1–6.
[22] M. E. Baran and F. F. Wu, "Network reconfiguration in distribution systems for loss reduction and load balancing," *IEEE Trans. Power Del.*, vol. 4, no. 2, pp. 1401–1407, Apr. 1989.
[23] C. C. Liu, S. J. Lee, and K. Vu, "Loss minimization for distribution feeders: Optimality and algorithms," *IEEE Trans. Power Del.*, vol. 4, no. 2, pp. 1281–1289, Apr. 1989.
[24] J. Olamaei, T. Niknam, and G. Gharehpetian, "Impact of distributed generators on distribution feeder reconfiguration," in *Proc. IEEE Lausanne Power Tech*, Lausanne, Switzerland, 2007, pp. 1747–1751.
[25] S. Yang, Q. Lei, F. Z. Peng, and Z. Qian, "A robust control scheme for grid-connected voltage-source inverter," *IEEE Trans. Ind. Electron.*, vol. 58, no. 1, pp. 202–212, Jan. 2011.
[26] J. He, Y. W. Li, and M. S. Munir, "A flexible harmonic control approach through voltage-controlled DG-grid interfacing converters," *IEEE Trans. Ind. Electron.*, vol. 59, no. 1, pp. 444–455, Jan. 2012.
[27] I.-Y. Chung, W. Liu, D. A. Cartes, E. G. Collins, and S. Moon, "Control methods of inverter-interfaced distributed generators in a microgrid system," *IEEE Trans. Ind. Electron.*, vol. 46, no. 3, pp. 1078–1088, May/Jun. 2010.
[28] C. A. Busada, S. G. Jorge, A. E. Leon, and J. A. Solsona, "Current controller based on reduced order generalized integrators for distributed generation systems," *IEEE Trans. Ind. Electron.*, vol. 59, no. 7, pp. 2898–2909, Jul. 2012.
[29] I. J. Balaguer, Q. Lei, S. Yang, U. Supatti, and F. Z. Peng, "Control for grid-connected and intentional islanding operations of distributed power generation," *IEEE Trans. Ind. Electron.*, vol. 58, no. 1, pp. 147–157, Jan. 2011.
[30] S. Alepuz, S. Busquets-Monge, J. Bordonau, J. Gago, D. González, and J. Balcells, "Interfacing renewable energy sources to the utility grid using a three-level inverter," *IEEE Trans. Ind. Electron.*, vol. 53, no. 5, pp. 1504–1511, Oct. 2006.
[31] S. Rahmani, N. Mendalek, and K. Al-Haddad, "Experimental design of a nonlinear control technique for three-phase shunt active power filter," *IEEE Trans. Ind. Electron.*, vol. 57, no. 10, pp. 3364–3375, Oct. 2010.